

Supporting Information

Efficient Electrocatalytic N₂ Reduction on CoO Quantum Dots

Ke Chu ^{1*}, Ya-ping Liu ¹, Yu-biao Li ¹, Hu Zhang ², Ye Tian ³

¹ *School of Materials Science and Engineering, Lanzhou Jiaotong University, Lanzhou 730070, China*

² *School of Materials Science and Engineering, University of Science and Technology Beijing, Beijing, 200083, China*

³ *Department of Physics, College of Science, Hebei North University, Zhangjiakou 075000, Hebei, China*

*Corresponding author. E-mail address: chukelut@163.com (K. Chu)

Experimental section

Calculation details

DFT calculations were conducted using Cambridge sequential total energy package (CASTEP). The exchange correlation interaction was described by Perdew-Burke-Ernzerhof (PBE) functional within the framework of generalized gradient approximation (GGA) [1, 2]. A U parameter of 3.8 eV was applied for Co atoms in CoO. A Monkhorst mesh of $4 \times 3 \times 1$ was used in k -point sampling, and a cutoff energy of 650 eV was adopted to expand the electron wave functions. During the geometry optimization, the force and the energy were converged to 0.01 eV/Å and 2×10^{-6} eV/atom, respectively. The (200) and (111) surfaces of bulk CoO was modeled using $4 \times 4 \times 1$ supercell with 5 atomic-layer slabs, in which bottom three slabs were constrained and top two slabs were relaxed. A vacuum space of 20 Å was applied to separate adjacent slabs.

The adsorption energy (ΔE) is defined as[3]

$$\Delta E = E_{\text{ads/slab}} - E_{\text{ads}} - E_{\text{slab}} \quad (4)$$

where $E_{\text{ads/slab}}$, E_{ads} and E_{slab} are the total energies for adsorbed species on slab, adsorbed species and isolated slab, respectively.

The Gibbs free energy (ΔG) of the NRR intermediates is calculated as [3]:

$$\Delta G = \Delta E + \Delta ZPE - T\Delta S \quad (3)$$

where ΔE is the adsorption energy, ΔZPE is the zero point energy difference and $T\Delta S$ is the entropy difference between the gas phase and adsorbed state.

Synthesis of CoO QD/RGO

All the chemicals were used as received without further purification. In the synthesis of CoO QD/RGO, 5 mL of GO aqueous dispersion (4 mg mL⁻¹) and 10 mL of Co(Ac)₂ solution were mixed under ultrasonication for 1 h. The mixed suspension was frozen in liquid nitrogen immediately. The obtained bulk was freeze-dried to form the aerogel. After that, the aerogel was fired by a commercial lighter from one side, and the flame instantaneously self-propagated throughout the aerogel within one second. The obtained sample was washed with deionized water several times to

remove the unreacted $\text{Co}(\text{Ac})_2$. For comparison, the bare RGO (without loading CoO QDs) was prepared through the same procedure without the addition of $\text{Co}(\text{Ac})_2$.

Electrochemical measurements

Electrochemical measurements were performed with a standard three-electrode system at CHI-660E electrochemical workstation at ambient temperature and pressure. The graphite rod, Ag/AgCl and catalyst loaded on carbon paper (CP) were used as the counter electrode, reference electrode and working electrode, respectively. The working electrode was made by loading catalyst ink on CP ($1 \times 1 \text{ cm}^2$) and dried under ambient environment. The catalyst ink was prepared by ultrasonically dispersing 1 mg of catalyst in 105 μL of ethyl alcohol containing 5 μL of Nafion (5 wt%). Then, 30 μL of catalyst ink was drop-cast onto the CP and dried under ambient conditions. The NRR test was carried out using an H-type two-compartment electrochemical cell separated by Nafion 115 membrane. The Nafion membrane was pretreated by heating it in 5% H_2O_2 solution for 1 h, 0.5 M H_2SO_4 for 1 h and deionized water for 1 h in turn. All potentials were converted to reversible hydrogen electrode (RHE) with $E_{\text{RHE}} = E_{\text{Ag/AgCl}} + 0.197 + 0.059 \times \text{pH}$. Prior to NRR test, the electrolyte was purged with N_2 for 30 min.

Determination of NH_3

The concentration of produced NH_3 was quantitatively determined by an indophenol blue method[4, 5]. Briefly, 4 mL of electrolyte was removed from the electrochemical reaction vessel, followed by sequential addition of 50 μL of oxidizing solution containing NaOH (0.75 M) and NaClO ($\rho_{\text{Cl}} = \sim 4$), 500 μL of coloring solution containing 0.32 M NaOH and 0.4 M $\text{C}_7\text{H}_6\text{O}_3$, and 50 μL of catalyst solution containing 1 wt% $\text{C}_5\text{FeN}_6\text{Na}_2\text{O}$. After standing for 1 h, the UV-Vis absorption spectrum was measured and the concentration-absorbance curves were calibrated by standard NH_4Cl solution with a series of concentrations (Fig. S10a), showing a good linear relation of absorbance value with NH_3 concentrations (Fig. S10b, $y=0.509x+0.051$, $R^2=0.995$).

NH_3 yield was calculated by

$$\text{NH}_3 \text{ yield} = \frac{C_{\text{NH}_3} \times V}{t \times m} \quad (1)$$

Faradaic efficiency (FE) was calculated by

$$\text{FE} = \frac{3 \times c_{\text{NH}_3} \times F \times V}{17 \times Q} \times 100\% \quad (2)$$

where F is the Faraday constant, c_{NH_3} is the measured NH_3 concentration, V is the volume of the electrolyte for NH_3 collection, t is the potential applied time, m is the mass loading of catalyst on CP and Q is the quantity of applied electricity.

Determination of N_2H_4

The N_2H_4 concentration was quantitatively determined by a method of Watt and Chrisp[5, 6]. In brief, 5 mL of electrolyte was removed from the electrochemical reaction vessel, followed by addition of 5 mL of a color reagent (mixture of 300 mL of ethyl alcohol, 5.99 g $\text{C}_9\text{H}_{11}\text{NO}$ and 30 mL of HCl) and stirring for 10 min. The UV-vis absorbance spectrum of the resulting solution was measured at a wavelength of 460 nm. The concentration-absorbance curves were calibrated by standard $\text{N}_2\text{H}_4 \cdot \text{H}_2\text{O}$ solution with a series of concentrations (Fig. S11a), showing a good linear relation of absorbance value with N_2H_4 concentrations (Fig. S11b, $y=0.634x+0.027$, $R^2=0.997$).

Characterizations

Transmission electron microscopy (TEM), high resolution transmission electron microscopy (HRTEM), high angle annular dark field (HAADF)-scanning transmission electron microscopy (STEM), energy-dispersive X-ray (EDX) and selected area electron diffraction (SAED) were carried out on a Tecnai G² F20 microscope. X-ray diffraction (XRD) pattern was conducted on a Shimadzu 7000LX diffractometer with Cu-K α radiation. Raman spectra were conducted on a Raman spectroscope (JY-HR800). X-ray photoelectron spectroscopy (XPS) analysis was recorded on a PHI 5702 spectrometer. Thermogravimetry (TG) analysis was performed on a Perkin-Elmer TGA7 instrument. ¹H NMR spectra were recorded on a 500 MHz Bruker superconducting-magnet nuclear magnetic resonance (NMR) spectrometer.

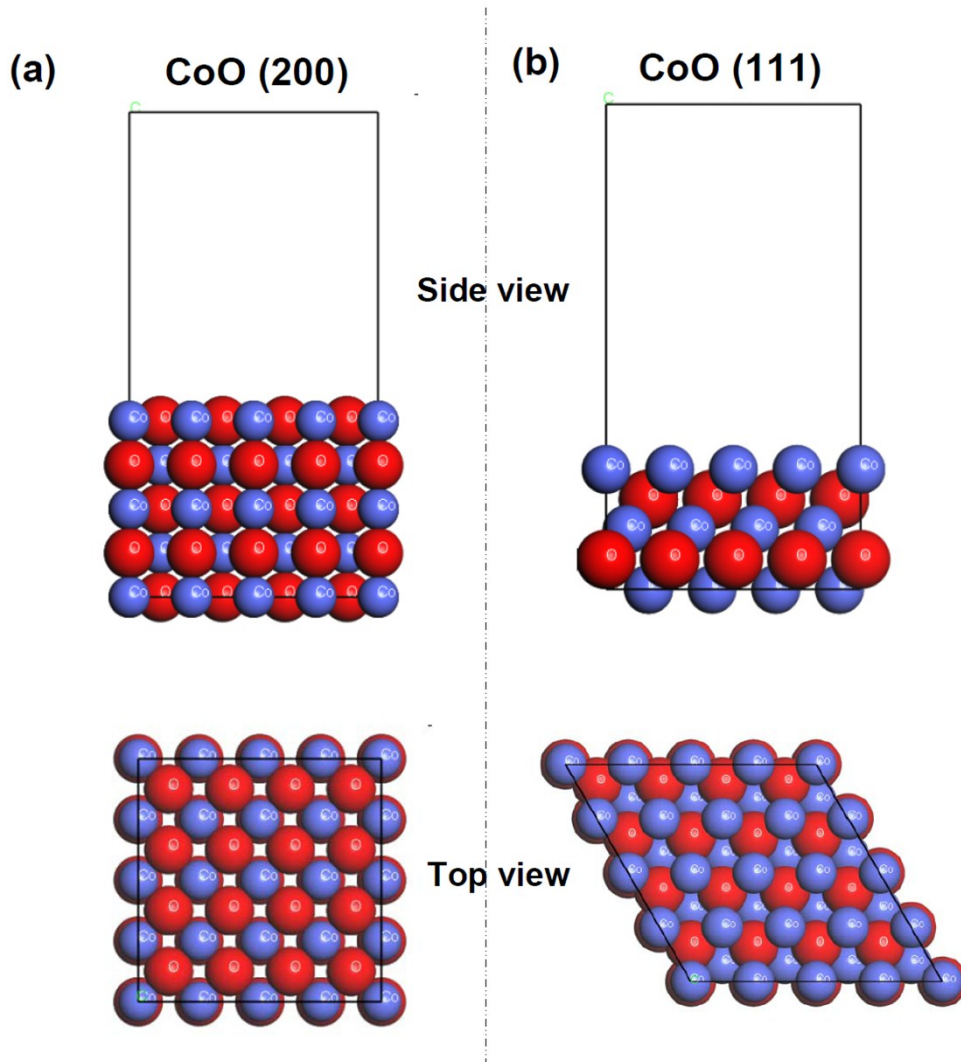


Fig. S1. Side-view and top-view images of CoO(200) and CoO(111) supercells. Lavender and red spheres are Co and O atoms, respectively.

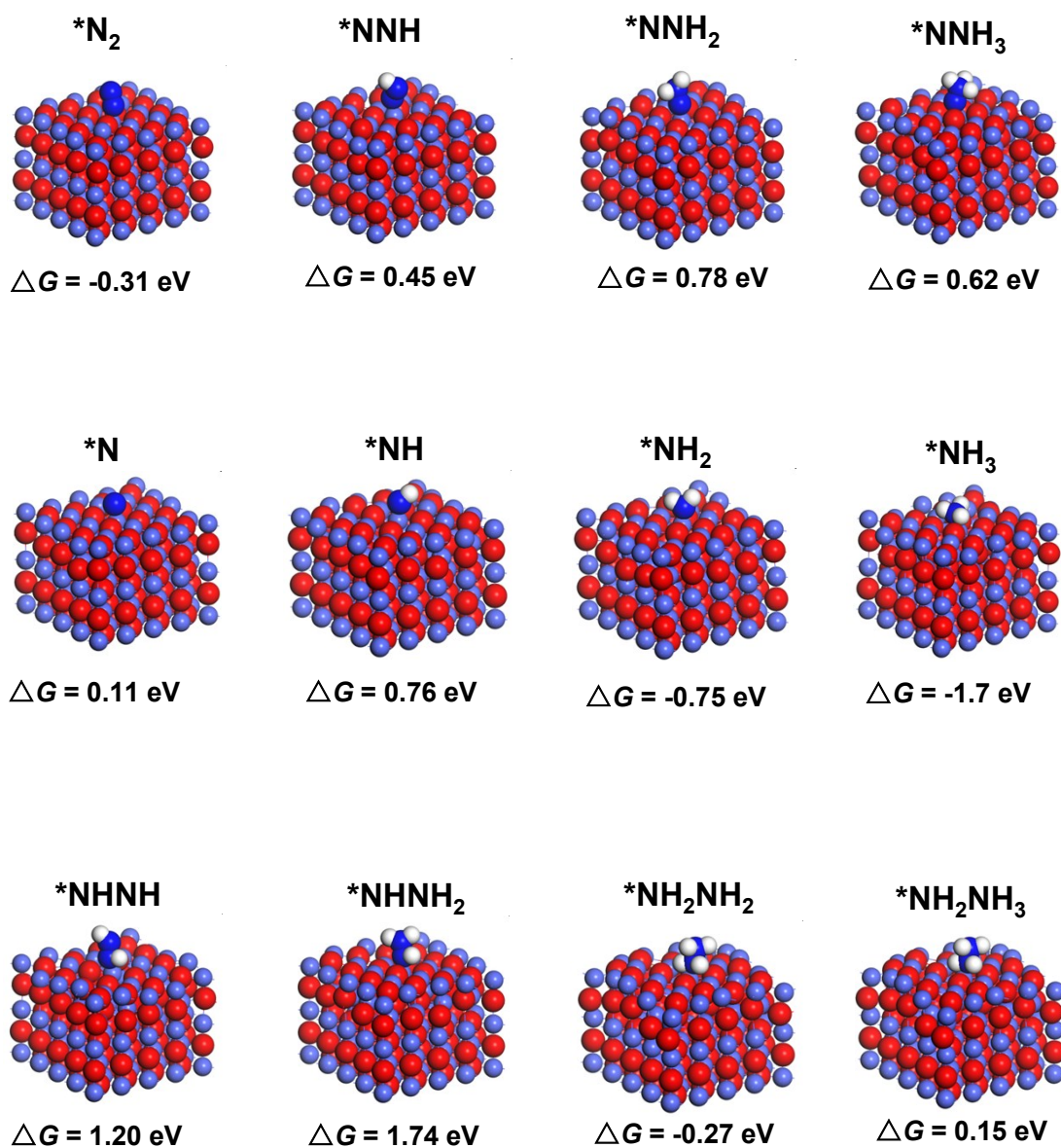


Fig. S2. Optimized configurations and calculated ΔG of all the reaction intermediates formed in distal and alternating associative pathways on CoO(200). Blue, lavender, red and white spheres are N, Co, O and H atoms, respectively.

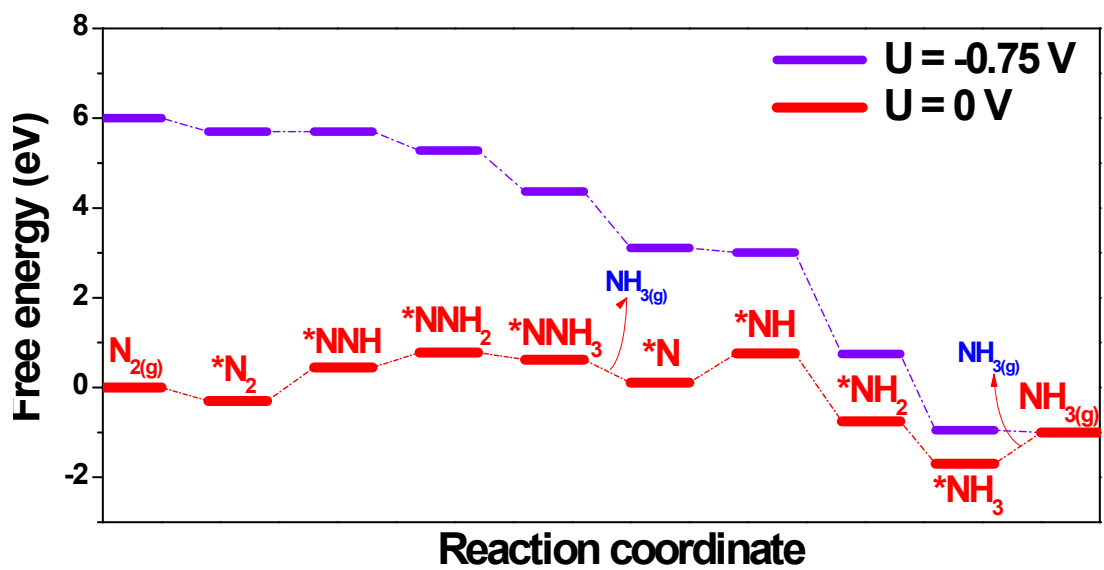


Fig. S3. Free energy diagrams of distal NRR pathway on CoO (200) at zero and applied energy of -0.75 V.

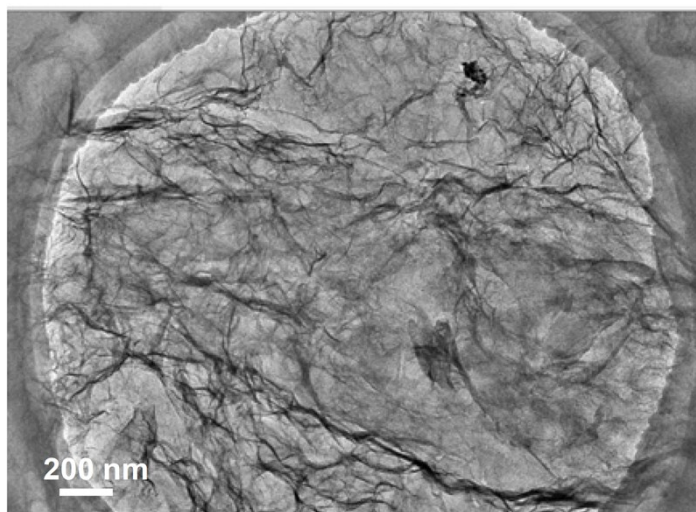


Fig. S4. Macroscopic TEM image of bare RGO.

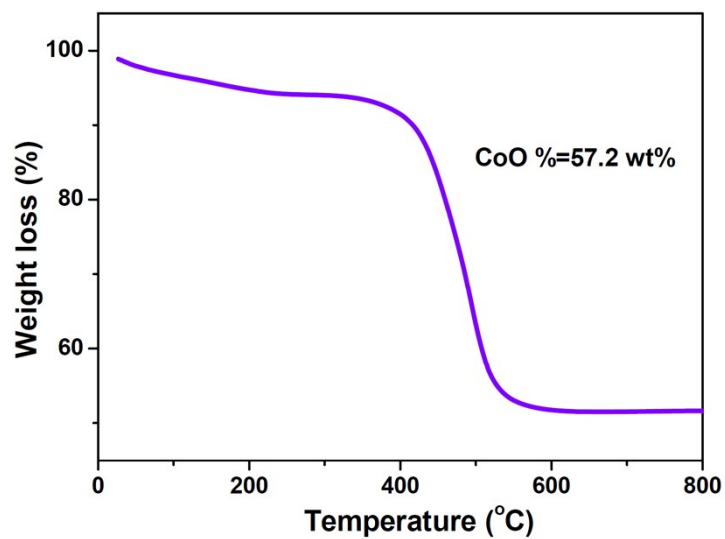


Fig. S5. TG curve of CoO QD/RGO at the heating rate of 5 °C/min under air atmosphere. The weight loss below 200 °C stems from the evaporation of moisture.

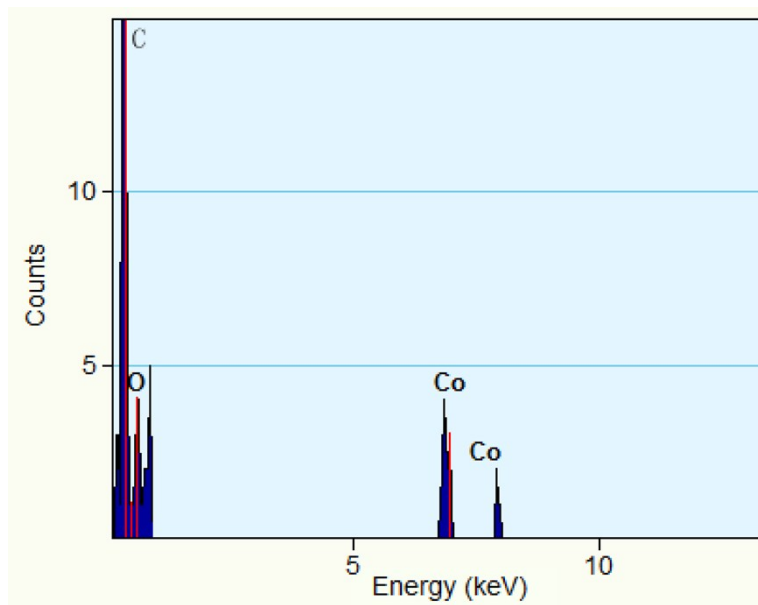


Fig. S6. EDX element analysis of CoO QD/RGO.

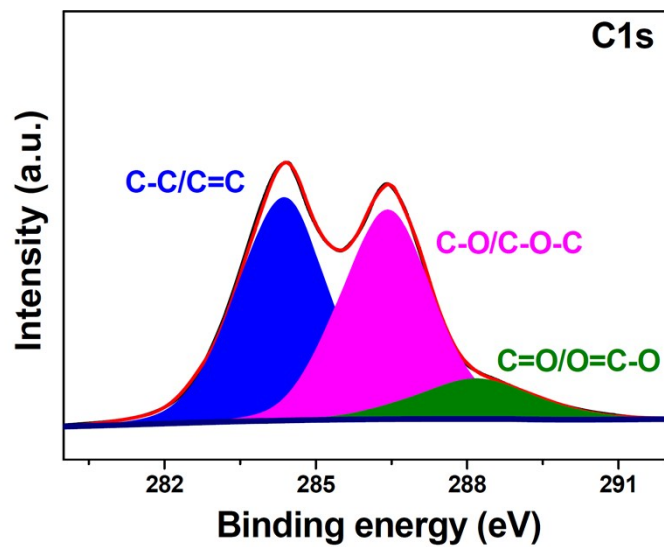


Fig. S7. XPS C1s spectra of pristine GO.



Fig. S8. Schematic of H-type electrochemical setup.

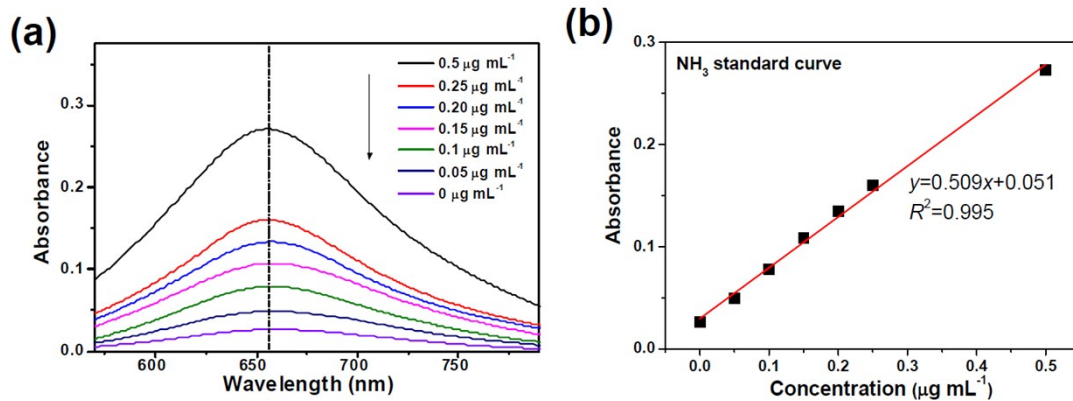


Fig. S9. (a) UV-Vis absorption spectra of indophenol assays with NH_4Cl after incubated for 2 h at ambient conditions. (b) Calibration curve used for calculation of NH_3 concentrations.

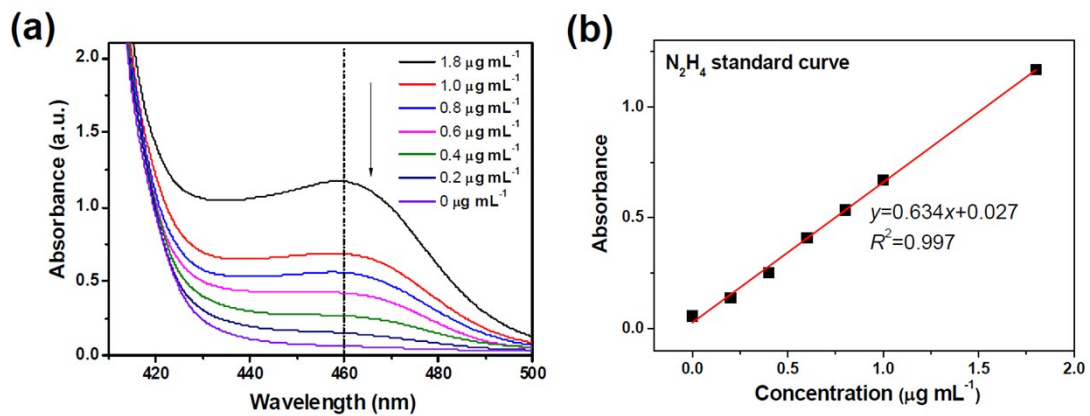


Fig. S10. (a) UV-Vis absorption spectra of N_2H_4 assays after incubated for 20 min at ambient conditions. (b) Calibration curve used for calculation of N_2H_4 concentrations.

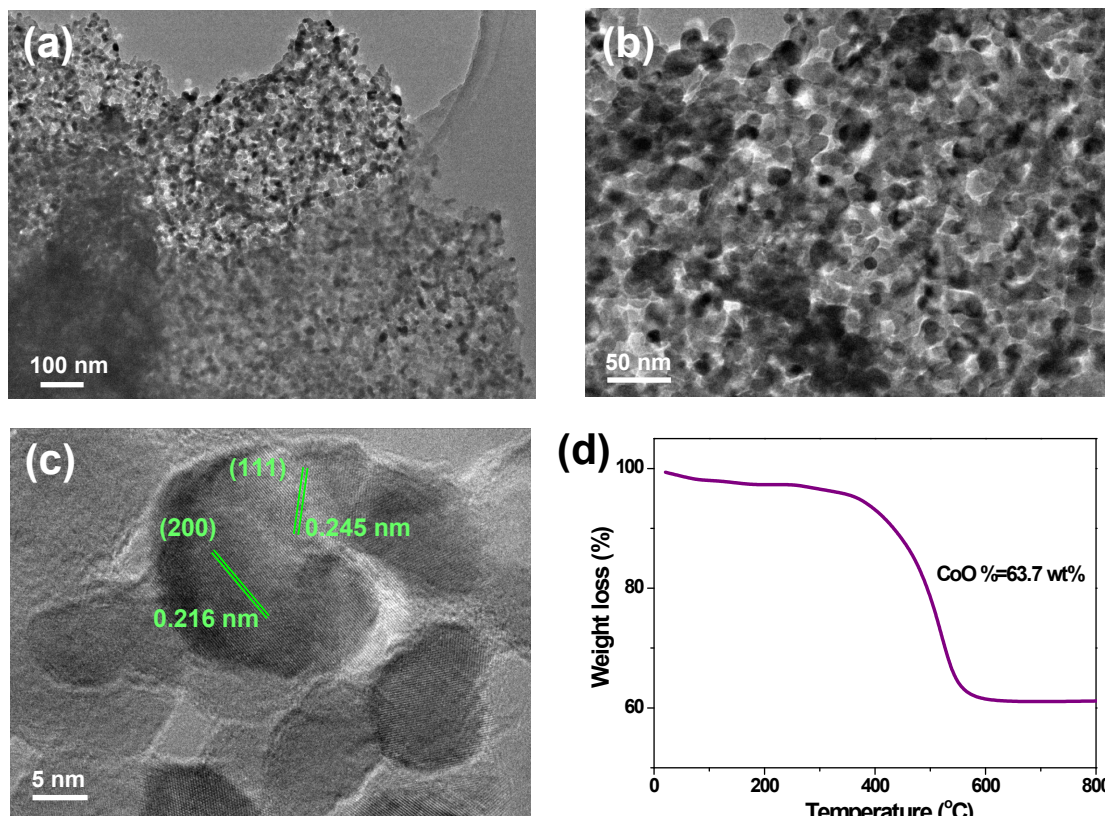


Fig. S11. (a, b) TEM images of CoO NP/RGO prepared by a hydrothermal method with a slight modification[7]. (c) HRTEM image of obtained CoO NP/RGO. (d) TG curve of CoO NP/RGO at the heating rate of 5 °C/min under air atmosphere.

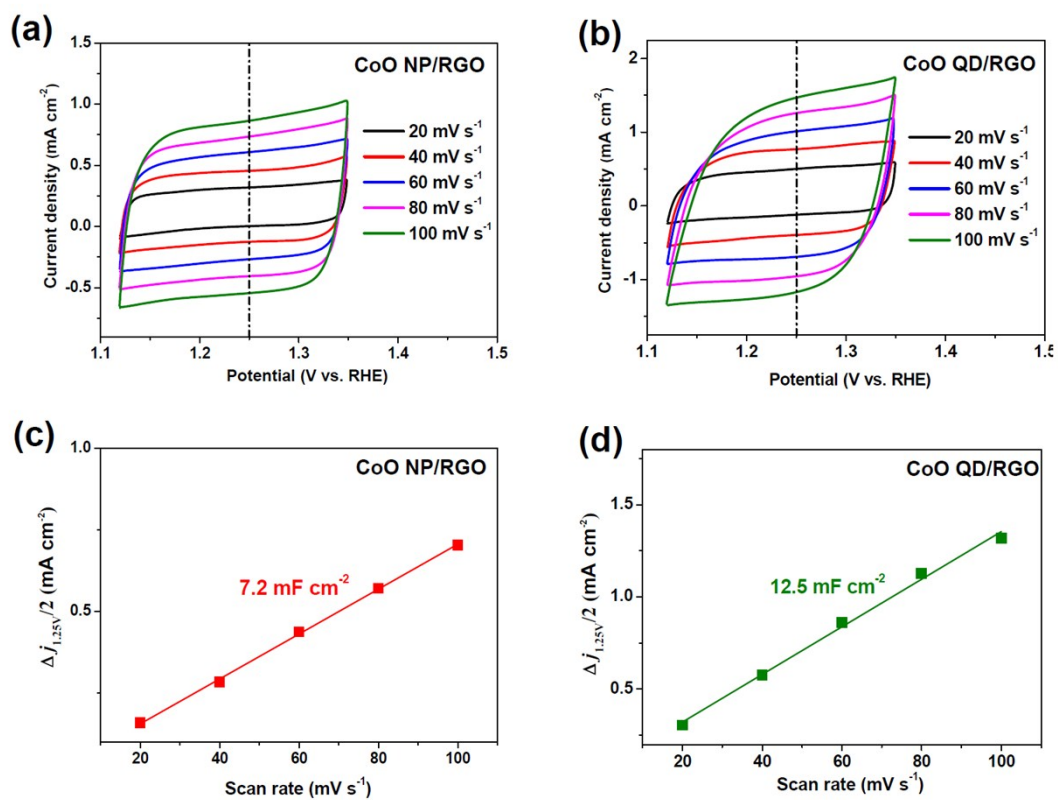


Fig. S12. CV curves of (a) CoO NP/RGO and (b) CoO QD/RGO at various scan rates of 20-200 mV s⁻¹, and corresponding plots of current density differences ($\Delta j/2$) vs. scan rate at 1.25 V vs. RHE.

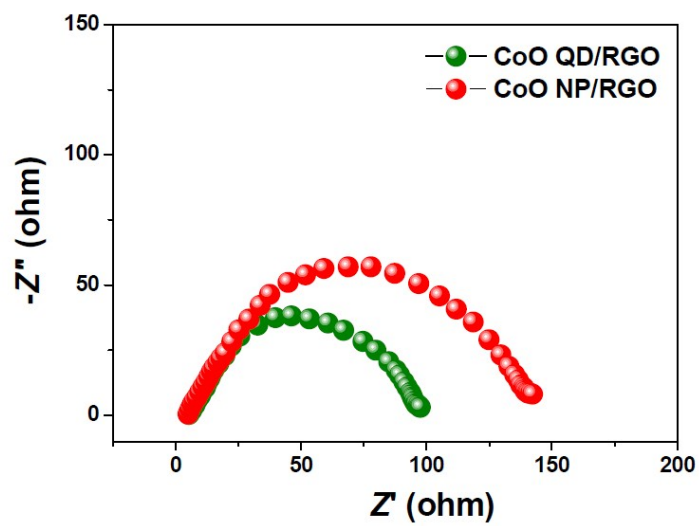


Fig. S13. Electrochemical impedance spectra of CoO QD/RGO and CoO NP/RGO.

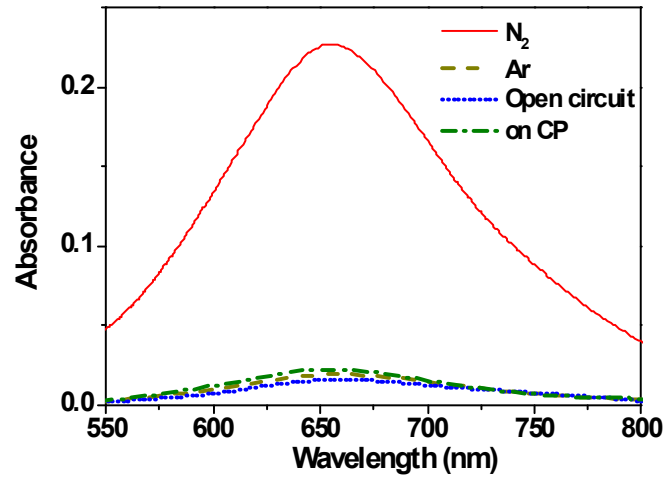


Fig. S14. UV-Vis absorption spectra of the electrolytes stained with indophenol indicator after 2 h electrolysis on CoO QD/RGO in N₂-saturated solution, Ar-saturated solutions, N₂-saturated solution at open circuit and N₂-saturated solution on pristine CP.

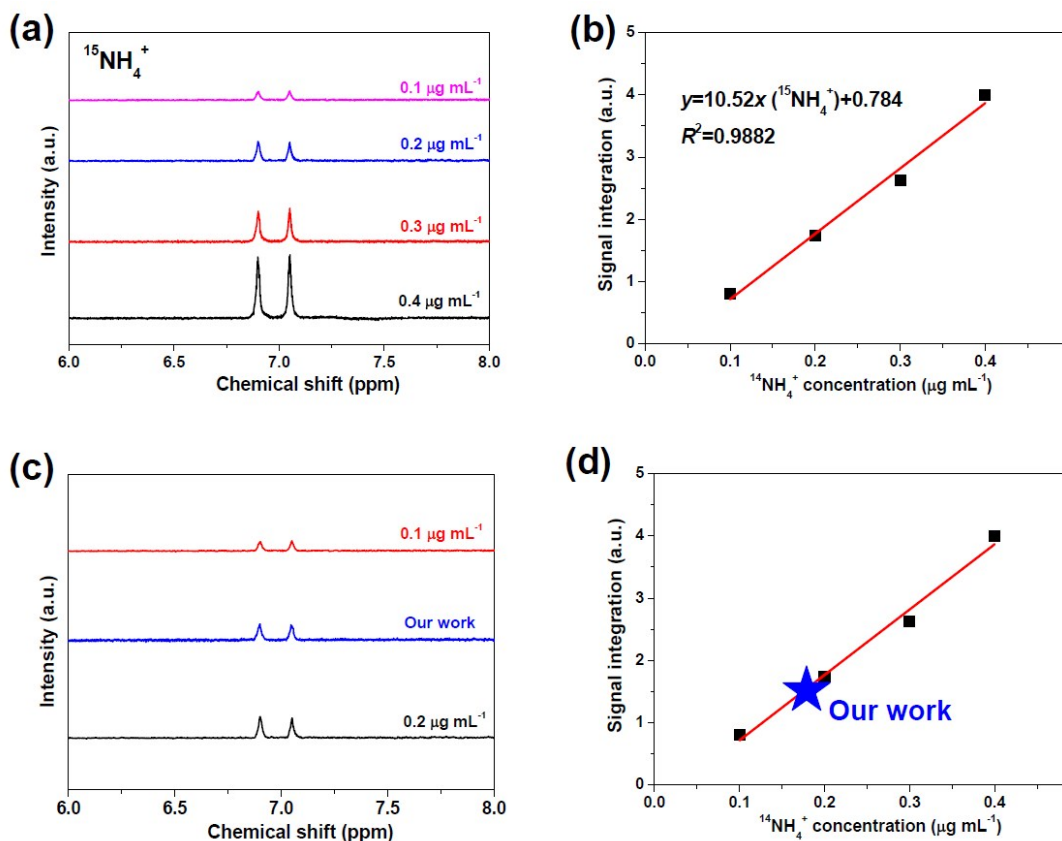


Fig. S15. (a) ^1H NMR spectra of $^{15}\text{NH}_4^+$ standard samples with different concentrations. (b) The corresponding calibration curve of $^{15}\text{NH}_4^+$ concentration vs. peak area intensity of NMR spectra. (c) NMR spectra of the electrolytes after catalyzing on CoO QD/RGO at -0.6 V for 1 h and $^{15}\text{NH}_4^+$ standard samples with $0.1 \mu\text{g mL}^{-1}$ and $0.2 \mu\text{g mL}^{-1}$. (d) The $^{15}\text{NH}_4^+$ concentrations of electrolytes quantitatively determined by the calibration curve (b).

It is well established that the peak area of NMR spectra is correlated to the NH_3 concentration, and thus the NH_3 concentration can be quantitatively determined by the NMR test [8, 9]. It is shown in Fig. S15b that the peak areas exhibit a good linear relation with $^{15}\text{NH}_4^+$ concentrations of standard samples. As shown in Fig. S15d, the measured sample shows the $^{15}\text{NH}_4^+$ concentration of $0.178 \mu\text{g mL}^{-1}$, which is very close to $0.172 \mu\text{g mL}^{-1}$ measured by the indophenol blue method, proving that the detected NH_3 stems from the NRR.

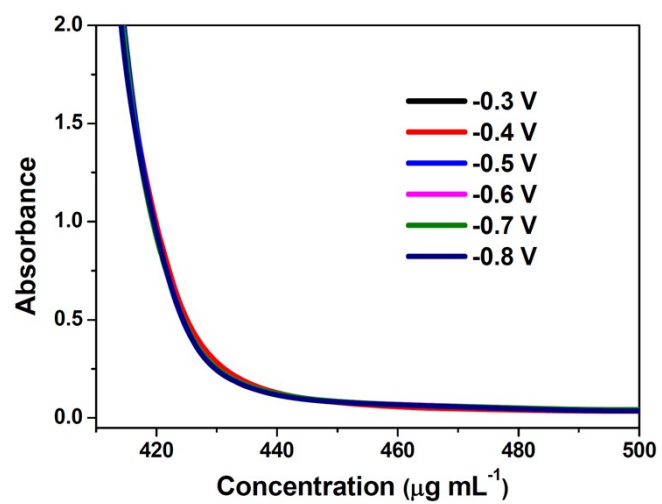


Fig. S16. UV-Vis spectra of the electrolyte (estimated by the method of Watt and Chrisp) at various potentials after 2 h electrocatalysis.

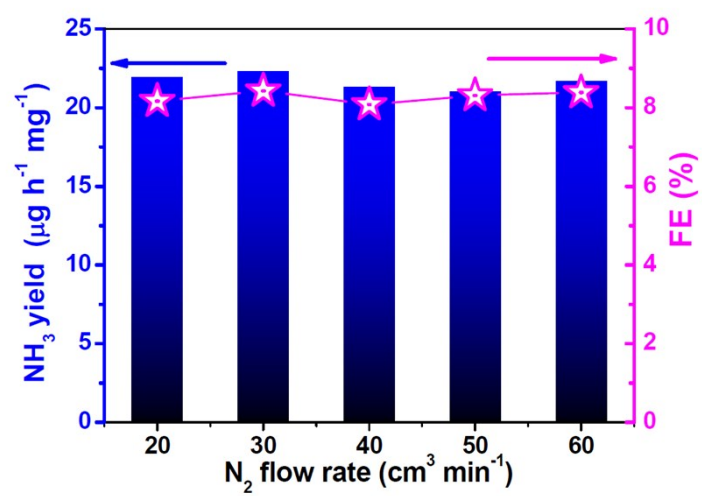


Fig. S17. NH₃ yields and FEs of CoO QD/RGO at various N₂ flow rates.

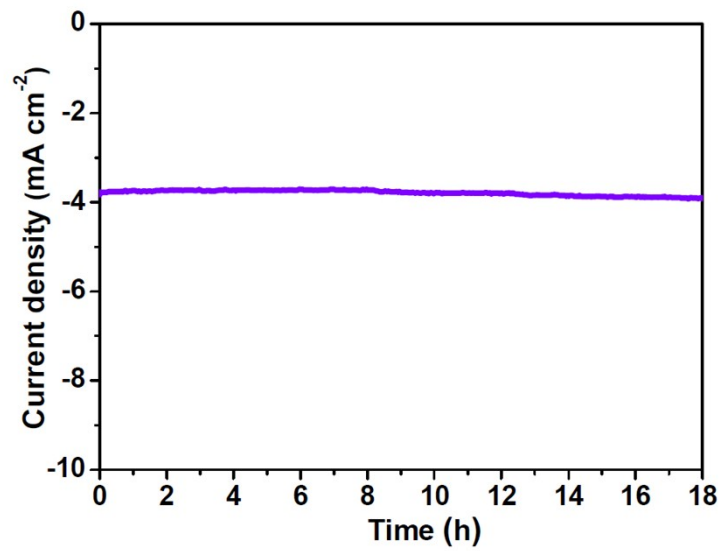


Fig. S18. Chronoamperometry test for 18 h electrolysis at -0.6 V.

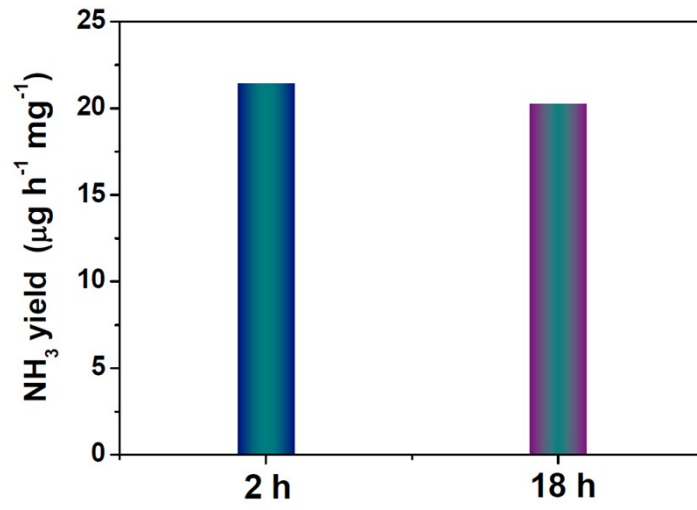


Fig. S19. NH₃ yields of CoO QD/RGO after 2 h and 18 h electrolysis

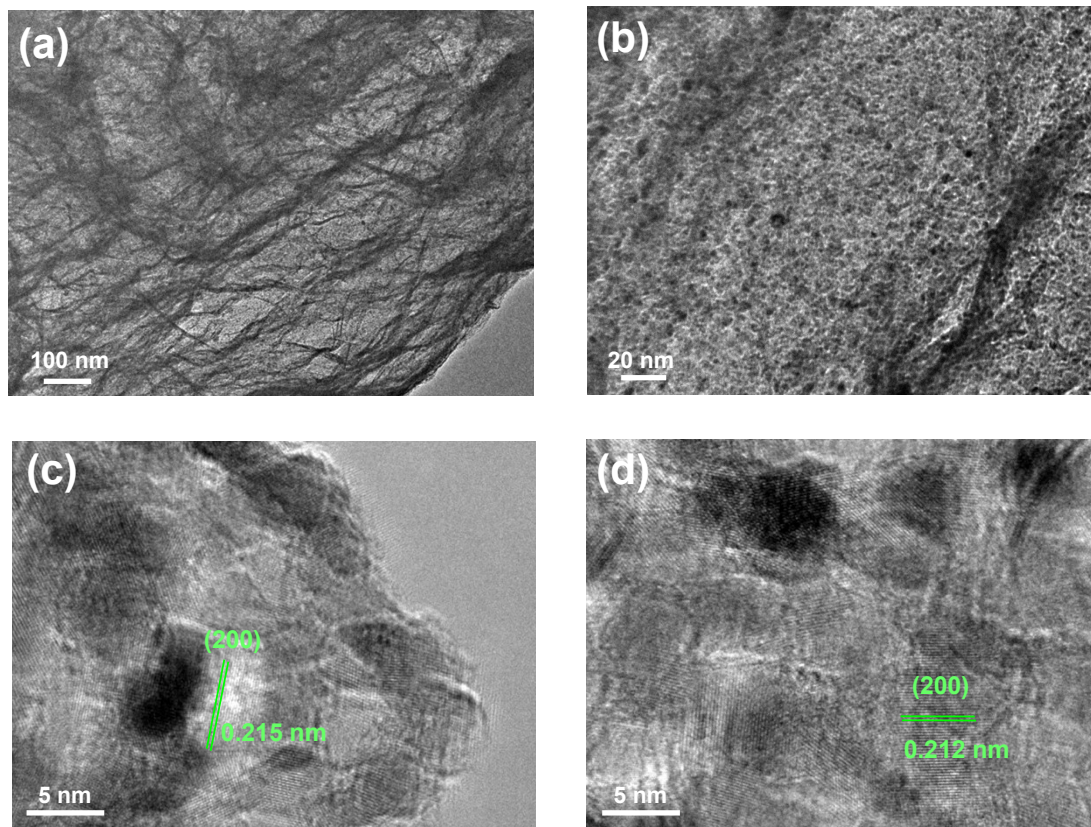


Fig. S20. Morphologies of CoO QD/RGO after stability test.

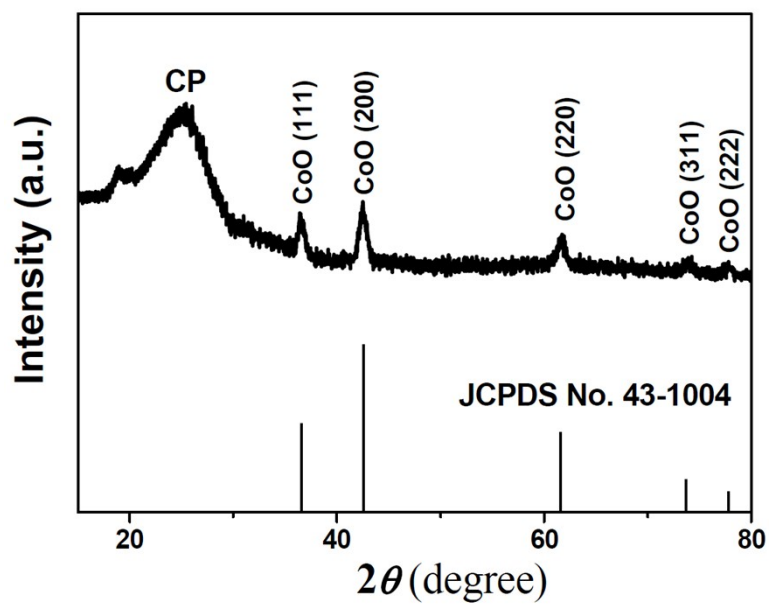


Fig. S21. XRD pattern of CoO QD/RGO after stability test.

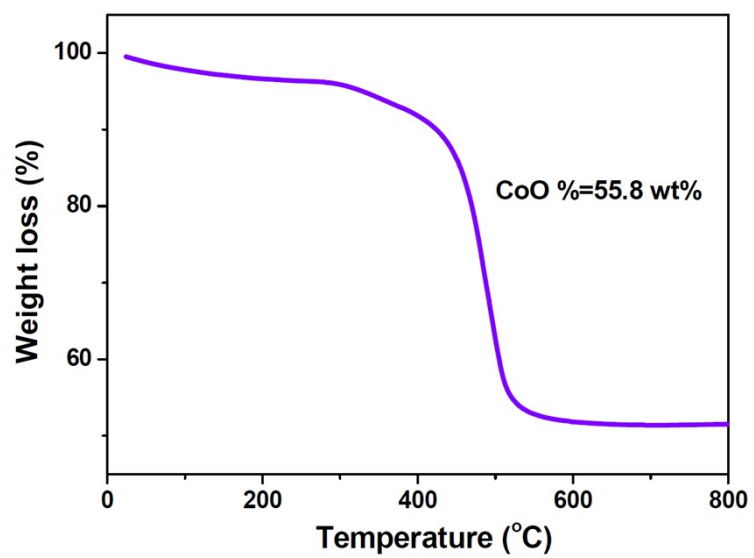


Fig. S22. TG curve of CoO QD/RGO after stability test.

Table S1. Comparison of NH₃ yield and Faradic efficiency (FE) of recently reported noble-metal and non-noble-metal electrocatalysts at ambient conditions

Catalyst	Electrolyte	Determination method	Potential (V vs RHE)	NH ₃ yield	FE (%)	Ref.
Au nanorods	0.1 M KOH	Nessler's reagent method	-0.2	1.65 $\mu\text{g cm}^{-2} \text{h}^{-1}$	4.02	[10]
BiVO ₄	0.2 M Na ₂ SO ₄	Indophenol blue method	-0.5	8.6 $\mu\text{g h}^{-1} \text{mg}^{-1}$	10.4	[11]
Au/CeO _x -RGO	0.1 M KOH	Salicylate method	-0.2	8.31 $\mu\text{g h}^{-1} \text{mg}^{-1}$	10.1	[12]
Au-TiO ₂ sub-nanocluster	0.1 M HCl	Indophenol blue method	-0.2	21.4 $\mu\text{g h}^{-1} \text{mg}^{-1}$	8.11	[13]
Mo ₂ C/C	0.5 M Li ₂ SO ₄	Nessler's reagent method	-0.3	11.3 $\mu\text{g h}^{-1} \text{mg}^{-1}$	7.8	[8]
MXene (Ti ₃ C ₂ T _x nanosheets)	0.5 M Li ₂ SO ₄	Nessler's reagent method	-0.1	4.7 $\mu\text{g cm}^{-2} \text{h}^{-1}$	5.78	[14]
PEBCD/C	0.5 M Li ₂ SO ₄	Nessler's reagent method	-0.5	1.58 $\mu\text{g cm}^{-2} \text{h}^{-1}$	2.85	[15]
Mo nanofilm	H ₂ O	Indophenol blue method	-0.49	$3.09 \times 10^{-11} \text{ mol s}^{-1} \text{ cm}^{-2}$	0.72	[16]
Hollow Au nanocages	0.5 M LiClO ₄	Indophenol blue method	-0.4	3.98 $\mu\text{g cm}^{-2} \text{h}^{-1}$	30.2	[17]
α -Fe@Fe ₃ O ₄	[C4mpyr] [eFAP]	Indophenol blue method	-0.23	$2.35 \times 10^{-11} \text{ mol s}^{-1} \text{ cm}^{-2}$	32	[18]
Fe ₂ O ₃ -CNT	0.50 M KOH	Salicylate method	-2	0.649 $\mu\text{g cm}^{-2} \text{h}^{-1}$	0.164	[19]
Pd/C	0.1 M PBS	Indophenol blue method	0.1	4.5 $\mu\text{g h}^{-1} \text{mg}^{-1}$	8.2	[20]
Bi ₄ V ₂ O ₁₁ -CeO ₂ nanofibers	0.1 M HCl	Indophenol blue method	-0.2	23.21 $\mu\text{g h}^{-1} \text{mg}^{-1} \text{cat.}$	10.16	[21]
Au thin-film	0.1 M KOH	Indophenol blue method	-0.5	0.235 $\mu\text{g cm}^{-2} \text{h}^{-1}$	0.12	[22]
Rh nanosheets	0.1 M KOH	Phenolphosphorite method	-0.2	23.88 $\mu\text{g h}^{-1} \text{mg}^{-1}$	0.217	[23]
B-doped graphene	0.05 M H ₂ SO ₄	Indophenol blue method	-0.5	9.8 $\mu\text{g cm}^{-2} \text{h}^{-1}$	10.8	[24]
Disordered carbon	0.1 M KOH	Indophenol blue method	-0.3	9.22 $\text{mmol g}^{-1} \text{h}^{-1}$	10.2	[25]
Polymeric carbon nitride	0.1 M HCl	Indophenol blue method	-0.2	8.09 $\mu\text{g h}^{-1} \text{mg}^{-1}$	11.59	[26]
MoS ₂ nanosheet	0.1 M Na ₂ SO ₄	Indophenol blue method	-0.5	$8.08 \times 10^{-11} \text{ mol s}^{-1} \text{ cm}^{-2}$	1.17	[5]

MoN nanosheets	0.1 M HCl	Indophenol blue method	-0.3	3.01×10^{-10} $\text{mol s}^{-1} \text{cm}^{-2}$	1.15	[27]
TiO ₂ nanosheet arrays	0.1 M Na ₂ SO ₄	Indophenol blue method	-0.7	9.16×10^{-11} $\text{mol s}^{-1} \text{cm}^{-2}$	2.5	[28]
TiO ₂ /RGO	0.1 M Na ₂ SO ₄	Indophenol blue method	-0.9	15.13 $\mu\text{g h}^{-1} \text{mg}^{-1}$	3.3	[29]
VN nanosheets	0.1 M HCl	Indophenol blue method	-0.5	8.40×10^{-11} $\text{mol s}^{-1} \text{cm}^{-2}$	2.25	[30]
MnO particles	0.1 M Na ₂ SO ₄	Indophenol blue method	-0.39	7.92 $\mu\text{g h}^{-1} \text{mg}^{-1}$	8.02	[31]
Ti ₃ C ₂ T _x nanosheets	0.1 M HCl	Indophenol blue method	-0.4	20.4 $\mu\text{g h}^{-1} \text{mg}^{-1}$	9.3	[32]
S-doped carbon nanospheres	0.1 M Na ₂ SO ₄	Indophenol blue method	-0.7	19.07 $\mu\text{g h}^{-1} \text{mg}^{-1}$	7.47	[33]
C-doped TiO ₂ nanoparticles	0.1 M Na ₂ SO ₄	Indophenol blue method	-0.7	16.22 $\mu\text{g h}^{-1} \text{mg}^{-1}$	1.84	[34]
Boron-doped TiO ₂	0.1 M Na ₂ SO ₄	Indophenol blue method	-0.8	14.4 $\mu\text{g h}^{-1} \text{mg}^{-1}$	3.4	[35]
La ₂ O ₃ nanoplate	0.1 M Na ₂ SO ₄	Indophenol blue method	-0.8	17.04 $\mu\text{g h}^{-1} \text{mg}^{-1}$	4.76	[36]
CoO QDs	0.1 M Na ₂ SO ₄	Indophenol blue method	-0.6	21.5 $\mu\text{g h}^{-1} \text{mg}^{-1}$	8.3	This work

Supplementary references

- [1] D. R. Hamann, M. Schlüter and C. Chiang, *Phys. Rev. Lett.*, 1979, **43**, 1494-1497.
- [2] S. Grimme, J. Antony, S. Ehrlich and H. Krieg, *J. Chem. Phys.*, 2010, **132**, 154104.
- [3] A. A. Peterson, *Energy Environ. Sci.*, 2010, **3**, 1311-1315.
- [4] D. Zhu, L. Zhang, R. E. Ruther and R. J. Hamers, *Nat. Mater.*, 2013, **12**, 836.
- [5] L. Zhang, X. Ji, X. Ren, Y. Ma, X. Shi, Z. Tian, A. M. Asiri, L. Chen, B. Tang and X. Sun, *Adv. Mater.*, 2018, **30**, 1800191.
- [6] G. W. Watt and J. D. Chrisp, *Anal. Chem.*, 1952, **24**, 2006-2008.
- [7] L. Zhang, Z. Wang, H. Wang, K. Yang, L. Wang, X. Li, Y. Zhang and H. Dong, *J. Alloy. Compd.*, 2016, **656**, 278-283.
- [8] H. Cheng, L. X. Ding, G. F. Chen, L. Zhang, J. Xue and H. Wang, *Adv. Mater.*, 2018, **30**, 1803694.
- [9] L. Zhang, L.-X. Ding, G.-F. Chen, X. Yang and H. Wang, *Angew. Chem. Int. Edit.*, 2018.
- [10] D. Bao, Q. Zhang, F. L. Meng, H. X. Zhong, M. M. Shi, Y. Zhang, J. M. Yan, Q. Jiang and X. B. Zhang, *Adv. Mater.*, 2017, **29**, 1604799.
- [11] J. X. Yao, D. Bao, Q. Zhang, M. M. Shi, Y. Wang, R. Gao, J. M. Yan and Q. Jiang, *Small Methods*, 2018, 1800333.
- [12] S. J. Li, D. Bao, M. M. Shi, B. R. Wulan, J. M. Yan and Q. Jiang, *Adv. Mater.*, 2017, **29**, 1700001.
- [13] M. M. Shi, D. Bao, B. R. Wulan, Y. H. Li, Y. F. Zhang, J. M. Yan and Q. Jiang, *Adv. Mater.*, 2017, **29**, 1606550.

- [14] Y. Luo, G.-F. Chen, L. Ding, X. Chen, L.-X. Ding and H. Wang, *Joule*, 2018, **1**, 1-11.
- [15] G.-F. Chen, X. Cao, S. Wu, X. Zeng, L.-X. Ding, M. Zhu and H. Wang, *J. Am. Chem. Soc.*, 2017, **139**, 9771-9774.
- [16] D. Yang, T. Chen and Z. Wang, *J. Mater. Chem. A*, 2017, **5**, 18967-18971.
- [17] M. Nazemi, S. R. Panikkanvalappil and M. A. El-Sayed, *Nano Energy*, 2018, **49**, 316-323.
- [18] B. H. Suryanto, C. S. Kang, D. Wang, C. Xiao, F. Zhou, L. M. Azofra, L. Cavallo, X. Zhang and D. R. MacFarlane, *ACS Energy Lett.*, 2018, **3**, 1219-1224.
- [19] S. Chen, S. Perathoner, C. Ampelli, C. Mebrahtu, D. Su and G. Centi, *Angew. Chem. Int. Edit.*, 2017, **56**, 2699-2703.
- [20] J. Wang, L. Yu, L. Hu, G. Chen, H. Xin and X. Feng, *Nat. Commun.*, 2018, **9**, 1795.
- [21] C. Lv, C. Yan, G. Chen, Y. Ding, J. Sun, Y. Zhou and G. Yu, *Angew. Chem. Int. Edit.*, 2018, **130**, 6181-6184.
- [22] Y. Yao, S. Zhu, H. Wang, H. Li and M. Shao, *J. Am. Chem. Soc.*, 2018, **140**, 1496-1501.
- [23] H. M. Liu, S. H. Han, Y. Zhao, Y. Y. Zhu, X. L. Tian, J. H. Zeng, J. X. Jiang, B. Y. Xia and Y. Chen, *J. Mater. Chem. A*, 2018, **6**, 3211-3217.
- [24] X. Yu, P. Han, Z. Wei, L. Huang, Z. Gu, S. Peng, J. Ma and G. Zheng, *Joule*, 2018, **2**, 1610-1622.
- [25] S. Mukherjee, D. A. Cullen, S. Karakalos, K. Liu, H. Zhang, S. Zhao, H. Xu, K. L. More, G. Wang and G. Wu, *Nano Energy*, 2018, **48**, 217-226.
- [26] C. Lv, Y. Qian, C. Yan, Y. Ding, Y. Liu, G. Chen and G. Yu, *Angew. Chem. Int. Edit.*, 2018, **57**, 10246-10250.
- [27] L. Zhang, X. Ji, X. Ren, Y. Luo, X. Shi, A. M. Asiri, B. Zheng and X. Sun, *ACS Sustain. Chem. Eng.*, 2018, **6**, 9550-9554.
- [28] R. Zhang, X. Ren, X. Shi, F. Xie, B. Zheng, X. Guo and X. Sun, *ACS Appl. Mater. Inter.*, 2018, **10**, 28251-28255.
- [29] X. Zhang, Q. Liu, X. Shi, A. M. Asiri, Y. Luo, X. Sun and T. Li, *J. Mater. Chem. A*, 2018, **6**, 17303-17306.
- [30] R. Zhang, Y. Zhang, X. Ren, G. Cui, A. M. Asiri, B. Zheng and X. Sun, *ACS Sustain. Chem. Eng.*, 2018, **6**, 9545-9549.
- [31] Z. Wang, F. Gong, L. Zhang, R. Wang, L. Ji, Q. Liu, Y. Luo, H. Guo, Y. Li, P. Gao, X. Shi, B. Li, B. Tang and X. Sun, *Adv. Sci.*, 2018, 1801182.
- [32] J. Zhao, L. Zhang, X.-Y. Xie, X. Li, Y. Ma, Q. Liu, W.-h. Fang, X. Shi, G. Cui and X. Sun, *J. Mater. Chem. A*, 2018, **6**, 24031-24035.
- [33] L. Xia, X. Wu, Y. Wang, Z. Niu, Q. Liu, T. Li, X. Shi, A. M. Asiri and X. Sun, *Small Methods*, 2018, 1800251.
- [34] Y. Wang, Q. Pan, B. Zhong, Y. Luo, G. Cui, X.-D. Guo and X. Sun, *Nanoscale Adv.*, 2019.
- [35] Y. Wang, K. Jia, Q. Pan, Y. Xu, Q. Liu, G. Cui, X.-D. Guo and X. Sun, *ACS Sustain. Chem. Eng.*, 2018.
- [36] B. Xu, Z. Liu, W. Qiu, Q. Liu, X. Sun, G. Cui, Y. Wu and X. Xiong, *Electrochim. Acta*, 2018, **298**, 106-111.